Inorganic Chemistry

Article

pubs.acs.org/IC

Determinants of Fe^{2+} over M^{2+} (M = Mg, Mn, Zn) Selectivity in Non-Heme Iron Proteins

Todor Dudev* and Valia Nikolova

Faculty of Chemistry and Pharmacy, Sofia University "St. Kliment Ohridski", 1164 Sofia, Bulgaria

ABSTRACT: Iron cations are indispensable players in a number of vital biological processes such as respiration, cell division, nitrogen fixation, oxygen transport, nucleotide synthesis, oxidant protection, O_2 activation in the metabolism of various organic substrates, gene regulation, and protein structure stabilization. The basic mechanisms and factors governing the competition between Fe^{2+} and other metal species from the cellular fluids such as Mg^{2+}, Mn^{2+}, and Zn^{2+} are, however, not well understood, and several outstanding questions remain. (i) How does the Fe^{2+} binding site select the "right" cation and protect itself from attacks by other biogenic cations present in the surrounding milieu? (ii) Do the iron binding sites employ different selectivity strategies toward metal cations possessing different ligand affinities and cytosolic concentrations? (iii) What are the key determinants of metal selectivity in Fe^{2+} proteins? In this study, by employing density functional theory calculations combined with polarizable continuum model computations, we endeavor to address these questions by evaluating the thermodynamic outcome of the competition between Fe^{2+} and $Mg^{2+}/Mn^{2+}/Zn^{2+}$ in model non-heme mononuclear metal binding sites of various compositions and charge states. The present calculations, which are in line with available experimental data, shed light on the mechanism of Fe^{2+}–$Mg^{2+}/Mn^{2+}/Zn^{2+}$ competition in non-heme iron proteins and disclose the key factors governing the process.

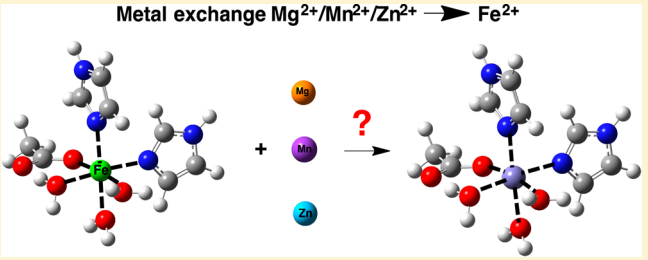

INTRODUCTION

Over the course of 2–3 billion years of cell evolution, about two dozen metal species have been selected and bestowed biological function ranging from enzyme catalysis to nucleic acid and protein structure stabilization, signal transduction, muscle contraction, hormone secretion, taste and pain sensation, blood coagulation, respiration, and photosynthesis.[1−5] They are the simplest, yet most versatile, participants in biochemical processes with a multitude of characteristic properties such as positive charge, flexible coordination sphere, specific ligand affinity and Lewis acidity, varying valence state and spin configuration, and specific mobility/diffusivity. The most abundant biogenic metal cations, chosen on the basis of their physicochemical properties and bioavailability, are Na^+, K^+, Mg^{2+}, Ca^{2+}, Zn^{2+}, Mn^{2+}, $Fe^{2+/3+}$, $Co^{2+/3+}$, Ni^{2+}, and $Cu^{+/2+}$.[1,3−5]

Iron, a redox-active element with oxidation state alternating between +2 and +3 (and sometimes +4), is an indispensable player in a number of vital biological processes such as respiration, cell division, nitrogen fixation, oxygen transport, nucleotide synthesis, oxidant protection, O_2 activation in the metabolism of various organic substrates, gene regulation, and protein structure stabilization.[6−8] Depending on the structure of the metal binding site, iron proteins can be classified into several groups: (1) heme proteins where the iron cation is coordinated to a heme porphyrin ring, which, on its side, is bound covalently or noncovalently to the host protein;[9] (2) iron–sulfur cluster proteins comprising [2Fe-2S], [3Fe-4S], and [4Fe-4S] clusters, embedded in the protein structure and coordinated to the protein, most often by Cys ligation to the cluster's iron atoms;[8] (3) mono- and polynuclear non-heme proteins possessing iron binding sites lined with amino acid residues donated by the host protein.[10−17] The composition of metal binding sites in representative mononuclear non-heme Fe^{2+} proteins is presented in Table 1. The data collected demonstrate that the preferred binding partners of Fe^{2+} are His and Asp^-/Glu^- side chains. The latter usually coordinate to the metal in a monodentate fashion. The typical Fe^{2+} binding site configuration is $His_2(Asp^-/Glu^-)_1$, denoted the "2-His-1-carboxylate facial triad motif".[11] It is a signature motif for a large group of iron dioxygenases, hydrolases, and synthases.[10−15] Other combinations between His and acidic residues exist as well: $His_1(Asp^-/Glu^-)_2$, $His_2(Asp^-/Glu^-)_2$, and $His_3(Asp^-/Glu^-)_1$. The coordination number of Fe^{2+} varies between 5 and 6 with water or substrate molecules complementing the coordination sphere.

Inside the cell, Fe^{2+} has to compete for protein binding sites with other biogenic metal species, such as Mg^{2+}, Mn^{2+}, and Zn^{2+}. Although these cations have the same charge and similar ionic radii (R_{Fe2+} = 0.78 Å, R_{Mg2+} = 0.72 Å, R_{Zn2+} = 0.74 Å, and R_{Mn2+} = 0.83 Å for hexacoordinated ions[20]), they possess different ligand affinities, as reflected in the Irving–Williams series:[21]

$$Mg^{2+} < Mn^{2+} < Fe^{2+} < Co^{2+} < Ni^{2+} < Cu^{2+} > Zn^{2+}$$

Received: July 28, 2016
Published: December 5, 2016

DOI: 10.1021/acs.inorgchem.6b01822
Inorg. Chem. 2016, 55, 12644–12650

Table 1. Composition of Fe^{2+} Binding Sites in Representative Mononuclear Non-Heme Proteins

protein	reference/ PDB entry	Fe^{2+}-binding ligands[a]
2,3-dihydroxybiphenyl dioxygenase	1KW3	H145, H209, E260, $2H_2O$
HPP dioxygenase	1CJX	H161, H240, E322, Sub^{bi}
homogentisate dioxygenase	1EY2	H335, $E341^{bi}$, H371, $2H_2O$
human factor inhibiting HIF	1MZF	H199, D201, H279, Sub^{bi}
human phenylalanine hydroxylase	1J8U	H285, H290, E330, $3H_2O$
homoprotocatechuate 2,3-dioxygenase	15	H155, H214, E267, Sub^{bi}
carbapenem synthase	11	H101, D103, H251, Sub^{bi}
clavaminate synthase	1DS1	H144, E146, H279, H_2O, Sub^{bi}
deacetoxycephalosporin C synthase	18	H183, D185, H243, H_2O, Sub^{bi}
isopenicillin N synthase	2IVI	H214, D216, H270, H_2O, Sub
extradiol dioxygenase	19	H146, H210, E260, $2H_2O$
TauD	1OS7	H99, D101, H255, Sub^{bi}
alkylsulfatase Atsk	1OII	H108, D110, H264, H_2O, Sub^{bi}
histone deacetylase 8	3MZ6	D178, H180, D267, $2H_2O$, Sub^{bi}
D-ribulose 5-phosphate 3-epimerase	3OVP	H35, D37, H70, D175, $2H_2O$
lipoxygenase	1F8N	H499, H504, H690, N694, $I839^{oxt}$, H_2O
5-methylcytosine deaminase	4R7W	H56, H58, H209, D308, Sub

[a]"Sub" stands for a substrate molecule. Residues/substrates with the superscript "'bi'" coordinate to the metal ion in a bidentate fashion. Monodentate binding is observed for other residues (with no superscript). The superscript "oxt" signifies an end carboxylate group. Water molecules within <3 Å of Fe^{2+} are assumed to be bound to the metal cation.

Magnesium and manganese ions, located at the far left-hand side of the series, have weaker ligand affinities than Fe^{2+}. Zinc cations, on the other side, exhibit much higher ligand coordinating strength than Fe^{2+} and form, as a rule, more stable complexes. Furthermore, these metal contenders are present in different free cytosolic concentrations ranging from millimolar for Mg^{2+} to micromolar for Fe^{2+} and Mn^{2+} and picomolar/femtomolar for Zn^{2+}.[22] Note that the respective concentrations in the resting cell generally correlate inversely with the Irving–Williams series: the greater the affinity of a cation for a given set of ligands, the lower its cytosolic concentration. Intriguing questions arise:

- How does the Fe^{2+} binding site select the "right" cation and protect itself from attacks by other biogenic cations (Mg^{2+}, Mn^{2+}, and Zn^{2+}) present in the cellular fluids?
- Do the iron binding sites employ different selectivity strategies toward metal cations possessing different ligand affinities and cytosolic concentrations?
- What are the key determinants of metal selectivity in Fe^{2+} proteins?

Here, we endeavor to address these questions by studying the thermodynamic outcome of the competition between Fe^{2+} and $Mg^{2+}/Mn^{2+}/Zn^{2+}$ in model non-heme mononuclear metal binding sites of various compositions and charge states (see Methods). Density functional theory (DFT) calculations in combination with polarizable continuum model (PCM) computations are employed. The Fe^{2+} binding site ion selectivity can be expressed in terms of the free energy, ΔG^{ε}, for replacing the "native" Fe^{2+} bound to the protein by its rival cation, M^{2+} (M = Mg, Mn, Zn):

$$[M^{2+}\text{-aq}] + [Fe^{2+}\text{-protein}] \rightarrow [M^{2+}\text{-protein}] + [Fe^{2+}\text{-aq}] \quad (1)$$

In eq 1, $[Fe^{2+}/M^{2+}\text{-protein}]$ and $[Fe^{2+}/M^{2+}\text{-aq}]$ represent the metal ion bound to protein ligands and unbound in the vicinity of the binding site, respectively. The binding cavity is characterized with an effective dielectric constant, ε, varying from ~4 for buried binding sites to ~30 for solvent-accessible binding pockets. A positive ΔG^{ε} implies a Fe^{2+}-selective site, whereas a negative value implies a M^{2+}-selective site. Our aim is to obtain reliable trends in the free energy changes with varying parameters of the system such as the structure, composition, overall charge, and solvent exposure of the metal binding site rather than reproduce the absolute ion exchange free energies in these metal centers. Notably, trends in the free energies computed using this approach have been found to be consistent with experimental observations in previous works.[23−33]

METHODS

Models Used. The side chains of Asp^-/Glu^- and His were modeled as acetate (CH_3COO^-) and imidazole ($C_3H_4N_2^0$), respectively. The metal cations under study (Fe^{2+}, Mg^{2+}, Mn^{2+}, and Zn^{2+}) are usually hexahydrated in aqueous solution.[34,35] Hence, their aqua complexes were modeled as $[M(H_2O)_6]^{2+}$ (M = Fe, Mg, Mn, Zn). In protein binding sites, Fe^{2+} is typically coordinated to five or six ligands[11,12] (see Table 1 as well). Accordingly, the respective five- and six-coordinated complexes were modeled as $\{[Fe(H_2O)_n(L)_{5-n}]\text{-}(H_2O)_p\}^{0/-}$ and $[Fe(H_2O)_n(L)_{6-n}]^{0/-}$, where L = CH_3COO^-, imidazole, n = 2, 3, and p = 0, 1. The structure of Fe^{2+} complexes was used as a starting point for geometry optimization of other metal complexes. The overall structure of the resulting Mg^{2+}, Mn^{2+}, and Zn^{2+} complexes did not change in the course of geometry optimization; thus, the coordination numbers of 5 and 6 were retained in the respective optimized structures. High-spin configurations for Fe^{2+} (quintuplet) and Mn^{2+} (sextuplet) were considered in line with the experimental and theoretical findings.[36,37]

DFT/PCM Calculations. The M06-2X method[38] in conjunction with the 6-311++G(d,p) basis set was employed to optimize the geometry of each metal complex in both the gas phase and condensed media and compute the electronic energies, E_{el}^{ε}, using the Gaussian 09 suite of programs.[39] Catalytic metal binding sites are located in cavities/crevices of the protein structure whose dielectric properties differ from that of the bulk water[40] and are comparable to those of the low-polarity solvents.[41] Thus, solution-phase computations were conducted in solvents mimicking the dielectric properties of buried and solvent-accessible binding sites: diethyl ether (ε = 4) and propanonitrile (ε = 29), respectively. Frequency calculations for each optimized structure were performed at the same M06-2X/6-311++G(d,p) level of theory. No imaginary frequency was found for any of the optimized structures. The frequencies were scaled by an empirical factor of 0.983[42] and used to compute the thermal energies, including zero-point energy, and entropies. The electronic energies in solution were corrected by performing single-point calculations on the respective fully optimized structures employing the SMD solvation model.[43] The differences $\Delta E_{el}^{\varepsilon}$, $\Delta E_{th}^{\varepsilon}$, and ΔS^{ε} between the products and reactants in eq 1 were used to calculate the metal exchange free energy at T = 298.15 K according to

$$\Delta G^{\varepsilon} = \Delta E_{el}^{\varepsilon} + \Delta E_{th}^{\varepsilon} - T\Delta S^{\varepsilon} \quad (2)$$

The basis set superposition error for this type of exchange reaction (eq 1) had been shown to be negligible[32,44] and was thus not considered in the present calculations.

The theoretical method and calculation protocol used were validated with respect to available experimental data and proven to be reliable, as they reproduced correctly the geometries of Mg^{2+}, Fe^{2+},

DOI: 10.1021/acs.inorgchem.6b01822
Inorg. Chem. 2016, 55, 12644−12650

Mn^{2+}, and Zn^{2+} representative structures as well as the free energies of $Mg^{2+}/Mn^{2+}/Zn^{2+} \rightarrow Fe^{2+}$ exchange in acetate, imidazole, and glycine complexes (Table 2).

Table 2. Comparison between Computed and Experimental Averaged Metal−Oxygen Bond Distances and Metal-Exchange Free Energies, ΔG^{78}, in M^{2+} (M = Mg, Fe, Mn, Zn) Complexes

complex or reaction	exptl	calcd
Metal−O (Å)		
$[Mg(H_2O)_6]^{2+}$	2.07 ± 0.03[a]	2.06
$[Zn(H_2O)_6]^{2+}$	2.08 ± 0.03[a]	2.11
$[Fe(H_2O)_6]^{2+}$	2.12/2.13[b]	2.15
$[Mn(H_2O)_6]^{2+}$	2.17−2.22[c]	2.19
ΔG^{78} (kcal/mol)		
$[Mg(H_2O)_6]^{2+} + [Fe(H_2O)_5(CH_3COO)_1]^{+} \rightarrow [Mg(H_2O)_5(CH_3COO)_1]^{+} + [Fe(H_2O)_6]^{2+}$	0.3[d]	1.8
$[Zn(H_2O)_6]^{2+} + [Fe(H_2O)_5(imidazole)_1]^{2+} \rightarrow [Zn(H_2O)_5(imidazole)_1]^{+} + [Fe(H_2O)_6]^{2+}$	−1.8[e]	−2.4
$[Mn(H_2O)_6]^{2+} + [Fe(H_2O)_5(imidazole)_1]^{2+} \rightarrow [Mn(H_2O)_5(imidazole)_1]^{+} + [Fe(H_2O)_6]^{2+}$	0.8[e]	2.6
$[Zn(H_2O)_6]^{2+} + [Fe(H_2O)_4(glycine)_1]^{2+} \rightarrow [Zn(H_2O)_4(glycine)_1]^{+} + [Fe(H_2O)_6]^{2+}$	−1.4[d]	−2.8
$[Mg(H_2O)_6]^{2+} + [Zn(H_2O)_4(glycine)_1]^{2+} \rightarrow [Mg(H_2O)_4(glycine)_1]^{+} + [Zn(H_2O)_6]^{2+}$	4.7[d]	4.8

[a]From ref 45. [b]From ref 46. [c]From ref 34. [d]Evaluated from the stability constants in water solution provided by ref 47. [e]Evaluated from the stability constants in water solution provided by ref 48.

RESULTS

2-His-1-Carboxylate Facial Triad Motif. A large group of mononuclear non-heme Fe^{2+} proteins possesses metal binding sites lined with two neutral His side chains and an anionic Asp^{-}/Glu^{-} residue ("2-His-1-carboxylate facial triad motif").[10−15] Since the coordination number of Fe^{2+} in these complexes is 5 or 6 (Table 1), we modeled both penta- and hexacoordinated Fe^{2+} binding sites comprising two imidazoles (model for His side chain), one acetate (model for Asp^{-}/Glu^{-} residues), and three water molecules (Figure 1). The three water ligands are directly bound to the metal cation in the hexacoordinated complex (Figure 1b), whereas one of them is transferred to the second coordination shell in the pentacoordinated counterpart (Figure 1a).

Figure 1 depicts the structures of penta- and hexacoordinated Fe^{2+} complexes along with the free energies of metal exchange $Mg^{2+}/Mn^{2+}/Zn^{2+} \rightarrow Fe^{2+}$ in the gas phase, ΔG^1, buried protein binding site, ΔG^4, and solvent-accessible metal center, ΔG^{29}. The results obtained reveal the following trends. (i) Mg^{2+} and Mn^{2+} cannot successfully compete with Fe^{2+} for the binding site, as evidenced by the positive free energies of metal substitution in both the gas phase and condensed media. This finding is not surprising in view of the weaker ligand affinities of Mg^{2+} and Mn^{2+} cations relative to those of the Fe^{2+} cation (see Introduction). However, Mn^{2+}, being closer in physicochemical properties to Fe^{2+} than Mg^{2+} to Fe^{2+}, is a more potent iron contender than Mg^{2+} (less positive free energies for the $Mn^{2+} \rightarrow Fe^{2+}$ exchange than for the $Mg^{2+} \rightarrow Fe^{2+}$ substitution). (ii) The Fe^{2+} binding sites are not well protected against attacks by the rival Zn^{2+} cations, which form more stable complexes and are able to displace Fe^{2+} from the respective metal centers (negative ΔG values for the $Zn^{2+} \rightarrow Fe^{2+}$ exchange in Figure 1). (iii) Solvation does not appear to be a major determinant of the Fe^{2+}/Mn^{2+} and Fe^{2+}/Zn^{2+} selectivity in these systems, as it only slightly affects the free energies of metal substitution and does not alter the trends observed in the gas phase. The effect is stronger for the Fe^{2+}/Mg^{2+} competition in pentacoordinated metal centers, where the increased solvent exposure of the binding site favors the Fe^{2+}/Mg^{2+} selectivity. (iv) Reducing the metal coordination number from 6 to 5 has a dual effect on the binding site selectivity: On one hand, it increases the Fe^{2+}/Mg^{2+} selectivity, as the pentacoordinated Mg^{2+} complex is less favored than its hexacoordinated counterpart (resulting in higher positive numbers for the Fe^{2+}/Mg^{2+} competition in the pentacoordinated complexes in Figure 1a than in the hexacoordinated structures in Figure 1b). On the other hand, however, it renders binding pockets less selective for Fe^{2+} over Zn^{2+}, since the Zn^{2+} binding is favorably affected by reducing the metal coordination number[49] (more negative ΔG values for the Fe^{2+}/Zn^{2+} competition in the pentacoordinated complexes in Figure 1a than for hexacoordinated constructs in Figure 1b).

The above findings apply to flexible Fe^{2+} binding sites that, in response to the specific physicochemical requirements of the guest noncognate metal, can readjust their structures upon replacing Fe^{2+} with $Mg^{2+}/Mn^{2+}/Zn^{2+}$, thus securing optimal accommodation for the incoming contender. Would, and if so, to what extent, the above trends change if the Fe^{2+} binding site were rigid and did not allow for any structural rearrangements of the protein ligands upon metal substitution? In addressing this question, we replaced Fe^{2+} with Mg^{2+}, Mn^{2+}, or Zn^{2+} in the Fe^{2+}-optimized Fe-3wat-2imi-1ace construct and performed partial geometry optimization of the resulting metal complex,

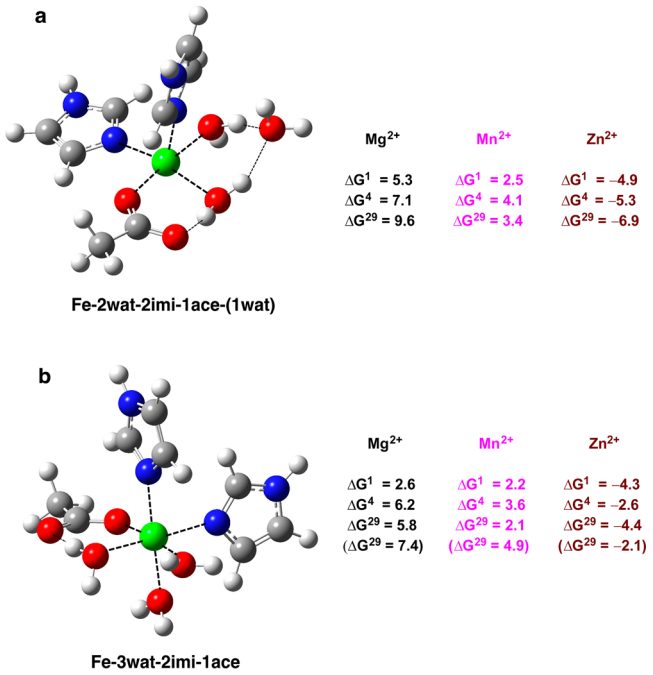

Figure 1. M06-2X/6-311++G(d,p) optimized structures of (a) pentacoordinated and (b) hexacoordinated Fe^{2+} model binding sites comprising two imidazole, one acetate, and three water ligands. The free energies ΔG^{ε} (in kcal/mol) for replacing Fe^{2+} in the binding site characterized by dielectric constant ε with M^{2+} (M = Mg, Mn, Zn) are shown on the right. ΔG^1 refers to cation exchange free energy in the gas phase, whereas ΔG^4 and ΔG^{29} refer to cation exchange free energies in an environment characterized by effective dielectric constants of 4 and 29, respectively. The free energies ΔG^{29}, evaluated for rigid Fe-3wat-2imi-1ace binding sites, are given in parentheses. Color scheme: Fe, green; O, red; N, blue; C, gray; H, light gray.

DOI: 10.1021/acs.inorgchem.6b01822
Inorg. Chem. 2016, 55, 12644−12650

keeping the positions of all protein ligands frozen (thus preserving the original cavity size unchanged) but allowing water molecules to reoptimize their positions. The electronic energies of the partially optimized structures were used in computing the $Mg^{2+}/Mn^{2+}/Zn^{2+} \rightarrow Fe^{2+}$ substitution free energies (numbers in parentheses in Figure 1b), which provide an upper limit of the rigidity effect on the metal selectivity in such inflexible non-heme binding sites. The results imply that rigidifying the metal binding site enhances the Fe^{2+} competitiveness over its non-native contenders (higher ΔG^{29} by ~2 kcal/mol), although it does not change the trends found for flexible metal centers (see above).

1-His-2-Carboxylate, 2-His-2-Carboxylate, and 3-His-1-Carboxylate Binding Sites. Other types of binding sites, comprising different combinations of His and carboxylate residues, were modeled as well (Figure 2). These mimic the Fe^{2+} active centers in histone deacetylase 8 $(His_1(Asp^-)_2$ binding site; Figure 2a), D-ribulose 5-phosphate 3-epimerase $(His_2(Asp^-)_2$ binding site; Figure 2b), and 5-methylcytosine deaminase $(His_3(Asp^-)_1$ binding site; Figure 2c).

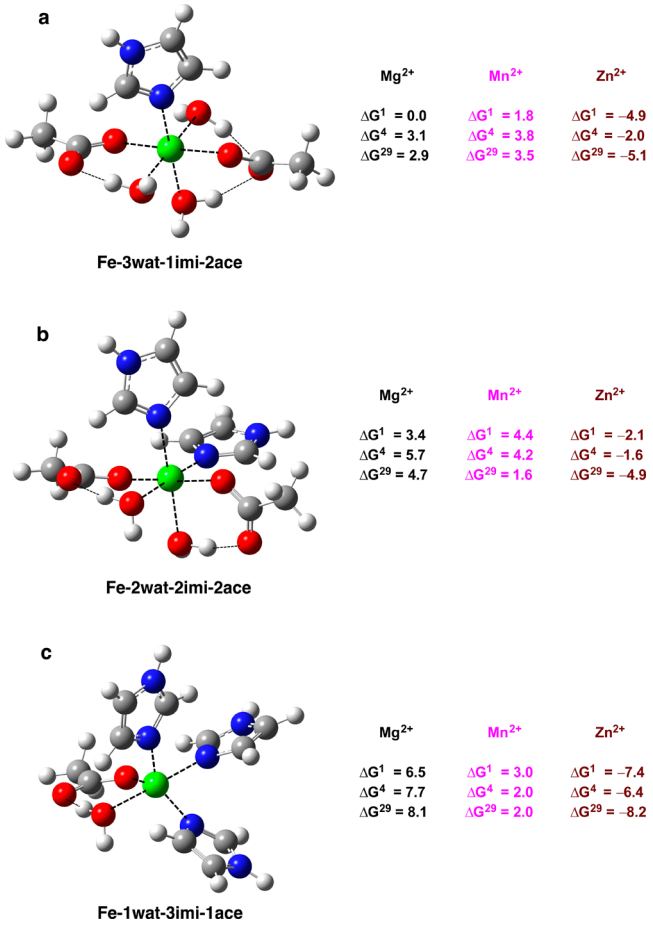

Figure 2. M06-2X/6-311++G(d,p) optimized structures of Fe^{2+} model binding sites comprising (a) one imidazole, two acetate, and three water ligands, (b) two imidazole, two acetate, and two water ligands, and (c) three imidazole, one acetate, and one water ligand. The free energies ΔG^{ε} (in kcal/mol) for replacing Fe^{2+} in the binding site characterized by dielectric constant ε with M^{2+} (M = Mg, Mn, Zn) are shown on the right. ΔG^1 refers to cation exchange free energy in the gas phase, whereas ΔG^4 and ΔG^{29} refer to cation exchange free energies in an environment characterized by effective dielectric constants of 4 and 29, respectively. Color scheme: Fe, green; O, red N, blue; C, gray; H, light gray.

In general, the trends in metal selectivity observed for this group of metal centers follow the tendencies found for the 2-His-1-carboxylate facial triad motif (see above): the binding sites are selective for Fe^{2+} over Mg^{2+} and Mn^{2+} (positive free energies for the $Mg^{2+} \rightarrow Fe^{2+}$ and $Mn^{2+} \rightarrow Fe^{2+}$ exchange; Figure 2) but are ill protected against $Zn^{2+} \rightarrow Fe^{2+}$ substitution (negative ΔG values for the respective reactions; Figure 2). Solvation has little effect on the process of metal competition.

The relative selectivity of these metal centers, however, varies with their structure and composition. Increasing the number of metal-coordinated imidazole ligands generally enhances the Fe^{2+} over Mg^{2+} selectivity. Thus, $\Delta G^{29}(Mg^{2+} \rightarrow Fe^{2+})$ increases from 2.9 kcal/mol in the Fe-3wat-*1imi*-2ace complex (Figure 2a) to 4.7 and 8.1 kcal/mol in Fe-2wat-*2imi*-2ace (Figure 2b) and Fe-1wat-*3imi*-1ace (Figure 2c) complexes, respectively. Reducing the Fe^{2+} coordination number to 5 in Fe-1wat-3imi-1ace also contributes to its enhanced selectivity over Mg^{2+}. Interestingly, alterations in the complex overall charge, related to the number of metal-bound anionic acetates, do not seem to significantly affect the metal selectivity in these systems. As seen, Fe-3wat-2imi-*1ace* with an overall charge of 1+ (Figure 1b) exhibits Fe^{2+}/Mg^{2+} and Fe^{2+}/Mn^{2+} selectivity in the protein environment very similar to that of Fe-2wat-2imi-*2ace* with an overall charge of 0 (Figure 2b). At the same time, Fe-3wat-1imi-*2ace* and Fe-2wat-2imi-*2ace* with the same overall charge of 0 are characterized with different metal selectivities (Figure 2a,b). Apparently, the imidazole ligand is more discriminative toward the metal species under study and plays a more substantial role in the selectivity process than its carboxylic counterpart. Furthermore, in analyzing the factors determining the Fe^{2+}/Zn^{2+} selectivity, the role of the binding site coordination geometry stands out. Octahedral binding sites (Fe-3wat-1imi-2ace and Fe-2wat-2imi-2ace, Figure 2a,b) are less Zn^{2+}/Fe^{2+} selective than pentacoordinated metal centers (Fe-1wat-3imi-1ace, Figure 2c), where lowering the metal coordination number from 6 to 5 favors Zn^{2+} binding to a greater extent than Fe^{2+} binding (more negative ΔG values in Figure 2c than in Figure 2a,b).

DISCUSSION

Central to the proper functioning of metalloproteins is their ability to select with high fidelity the "right" metal cation from the mixture of ions present in the surrounding fluids. Proteins have evolved different selectivity strategies enabling them to preferentially bind the cognate metal cation and protect the active site from attacks by unwanted, non-native contenders, which, if bound, may inactivate the host protein and disrupt the related biochemical reactions. A key selectivity strategy lies in the host protein itself, whose metal binding site features have been finely tuned to account for the subtle differences in the properties of the competing cations. Characteristics of the metal binding site such as its relative rigidity and solvent accessibility, as well as the type, charge, number, orientation, and protonation state of the metal-coordinating ligands, which determine the protein cavity size, geometry, and charge density, influence the metal ion selectivity.[22] In several cases, however, the host protein alone is not able to withstand attacks from other metal cations, which could displace the cognate metal cofactor from the binding site. In such circumstances, it is the cell machinery that orchestrates the selectivity process: metalloregulatory proteins tightly control metal homeostasis

DOI: 10.1021/acs.inorgchem.6b01822
Inorg. Chem. 2016, 55, 12644−12650

in living cells by keeping the concentrations of non-native, potentially damaging metal species sufficiently low in comparison to those of the native, less competitive cofactors.[22] Present DFT/PCM calculations shed light on the mechanism of the Fe^{2+}–M^{2+} (M = Mg, Mn, Zn) competition in non-heme iron binding sites and disclose the key factors governing the process.

Fe^{2+}–Mg^{2+} Competition. The results obtained reveal that Mg^{2+} cannot successfully compete with Fe^{2+} for non-heme metal centers, evidenced by the high positive free energies evaluated for the $Mg^{2+} \rightarrow Fe^{2+}$ exchange (Figures 1 and 2). The major determinant of the high Fe^{2+}/Mg^{2+} selectivity in these systems is the composition of the active center, which is invariably lined with His amino acid residues. The "hard" (weakly polarizable) Mg^{2+} cation does not bind as favorably to the "borderline" (more polarizable) histidine residue as its "borderline" Fe^{2+} contender. The histidine residues appear to be more discriminative toward the two competing cations than the respective Asp^-/Glu^- ligands and could be considered as the selectivity bearers in these systems (see above). The Fe^{2+} selectivity of the binding site would be further increased if the metal center is rigid and five-coordinated, as opposed to six-coordinated, that substantially disfavors Mg^{2+} from binding, which strongly prefers an octahedral arrangement in its complexes.

Fe^{2+}–Mn^{2+} Competition. Divalent manganese and iron cations are neighbors in the Irving–Williams series, possessing similar ligand affinities, ion radii, coordination preferences, and cytosolic concentrations, thus appearing to be almost equally strong competitors for protein binding sites. Our calculations reveal, not surprisingly, that iron centers, although still preferably binding Fe^{2+}, are weakly selective for Fe^{2+} over Mn^{2+} and are vulnerable to Mn^{2+} attacks. This is evidenced by positive, but low in absolute value, free energies (just a few kcal/mol) of the $Mn^{2+} \rightarrow Fe^{2+}$ exchange in both the gas phase and protein environment (Figures 1 and 2). The poor Fe^{2+}/Mn^{2+} selectivity, resulting in an easily surmountable thermodynamic barrier for the $Mn^{2+} \rightarrow Fe^{2+}$ substitution, however, might be beneficial for the cell metabolism and/or survival. Under conditions of Fe^{2+} deprivation the iron protein may sequester Mn^{2+} cations from the surrounding milieu which, due to their close resemblance to the native Fe^{2+} ions, secure uninterrupted cell metabolism.[50,51] Furthermore, Mn^{2+} is not oxidizable and does not react with H_2O_2, whereas the "catalytic" Fe^{2+} is prone to oxidation by H_2O_2 (Fenton reaction), causing subsequent inactivation of the respective enzymes. Hence, under conditions of oxidative stress, the Mn^{2+}-loaded iron enzymes remain active. In such circumstances, the cell machinery comes into action, ensuring favorable conditions for Mn^{2+} binding by elevating its cytosolic concentration relative to that of Fe^{2+}.[52,53]

Fe^{2+}–Zn^{2+} Competition. A zinc cation, characterized by greater ligand affinity than Fe^{2+}, can outcompete a iron cation and displace it from its binding sites regardless of their composition and structure (negative free energies for the $Zn^{2+} \rightarrow Fe^{2+}$ substitution in the entire series of complexes; Figures 1 and 2). The present results are in line with a series of in vitro experiments showing that, indeed, Zn^{2+} binds to the protein with much greater affinity than Fe^{2+}.[54−58] Although the host protein preferentially binds Zn^{2+} in vitro, it is loaded and activated by Fe^{2+} in vivo.[54−59] Inside the cell, since the protein alone is not able to withstand the attacks by rival Zn^{2+}, it is the cell machinery which, by strictly controlling the metal homeostasis and maintaining the free Zn^{2+} concentration at very low levels (in the picomolar to femtomolar range[22]), turns the balance in favor of Fe^{2+}. It has been suggested, however, that in critical situations (oxidative stress or Fe^{2+} deficiency) the iron enzyme (which does not operate through a metal redox mechanism[60]) may bind and become activated by Zn^{2+}, thus warranting the cell survival.[56,57]

CONCLUSIONS

Various non-heme Fe^{2+} binding sites differing in structure, composition, rigidity, charge state, and solvent exposure have been modeled, and their metal selectivity has been assessed. The results obtained reveal three major factors governing the metal selectivity in these systems, whose interplay determines the outcome of the competition between Fe^{2+} and its contenders:

- the physicochemical properties of the metal cations themselves, reflected in the Irving–Williams series
- the properties of the protein binding site
- the free cytosolic concentration of the competing metal cations.

The present theoretical calculations in combination with available experimental data suggest a dual mechanism for metal selectivity in iron non-heme proteins including internal and external factors. With respect to Mg^{2+}, it is the protein itself that controls the selectivity process by suitably optimizing the parameters of its binding site. The structure, rigidity, and composition of the metal center, which are tuned in accordance with the physicochemical properties of the cognate Fe^{2+} cation, appear to be the key descriptors of the Fe^{2+}/Mg^{2+} selectivity in these systems. Thus, Fe^{2+} can outcompete Mg^{2+} despite the 3-fold higher free cytosolic concentration of the latter.[22] The iron binding sites are tuned to select Fe^{2+} over Mn^{2+} as well, although the Fe^{2+}/Mn^{2+} selectivity is lower than the Fe^{2+}/Mg^{2+} selectivity. In the competition between Fe^{2+} and strong transition metals, such as Zn^{2+}, however, the control is transferred to the cell machinery, which regulates the selectivity process. The key determinants of metal selectivity in this case are the free metal cytosolic concentrations, which, being tightly controlled by the synchronized action of a number of cell devises, can tilt the balance in favor of the less active "native" cation. Note that the host protein/cell may benefit from the poor or reversed Fe^{2+} selectivity with respect to transition metals (Mn^{2+} or Zn^{2+}), as these competitors could substitute for the native cofactor in case of Fe^{2+} deprivation or oxidative stress.

AUTHOR INFORMATION

Corresponding Author

*E-mail for T.D.: t.dudev@chem.uni-sofia.bg.

ORCID

Todor Dudev: 0000-0002-8186-2141

Notes

The authors declare no competing financial interest.

REFERENCES

(1) Frausto da Silva, J. J. R.; Williams, R. J. P. *The Biological Chemistry of the Elements*; Oxford University Press: Oxford, U.K., 1991.

(2) Lippard, S. J.; Berg, J. M. *Principles of Bioinorganic Chemistry*; University Science Books: Mill Valley, CA, 1994.

(3) Christianson, D. W.; Cox, J. D. Catalysis by Metal-activated Hydroxide in Zinc and Manganese Metalloenzymes. *Annu. Rev. Biochem.* **1999**, *68*, 33−57.

DOI: 10.1021/acs.inorgchem.6b01822
Inorg. Chem. 2016, 55, 12644−12650

(4) Bertini, I.; Sigel, A.; Sigel, H. *Handbook on Metalloproteins*; Marcel Dekker: New York, 2001.
(5) Williams, R. J. P. The Natural Selection of the Chemical Elements. *Cell. Mol. Life Sci.* **1997**, *53*, 816−829.
(6) Yee, G. M.; Tolman, W. B. Transition Metal Complexes and the Activation of Dioxygen. In *Sustaining Life on Planet Earth: Metalloenzymes Mastering Dioxygen and Other Chewy Gases*; Kroneck, P. M. H., Sosa Torres, M. E., Eds.; Springer: Berlin, 2015; Metal Ions in Life Sciences *15*, Chapter 5, pp 120−131.
(7) Elizabeth, C. T. In *Encyclopedia of Metalloproteins*; Uversky, V. N., Kretsinger, R. H., Permyakov, E. A., Eds.; Springer Science: New York, 2013; p 1032.
(8) Crain, A. V.; Duschene, K. S.; Peters, J. W.; Broderick, J. B. In *Encyclopedia of Metalloproteins*; Uversky, V. N., Kretsinger, R. H., Permyakov, E. A., Eds.; Springer Science: New York, 2013; pp 1034−1044.
(9) Poulos, T. L. Heme Enzyme Structure and Function. *Chem. Rev.* **2014**, *114*, 3919−3962.
(10) Hausinger, R. P. Fell/alpha-ketoglutarate-dependent Hydroxylases and Related Enzymes. *Crit. Rev. Biochem. Mol. Biol.* **2004**, *39*, 21−68.
(11) Costas, M.; Mehn, M. P.; Jensen, M. P.; Que, Jr. Dioxygen Activation at Mononuclear Non-heme Iron Active Sites: Enzymes, Models and Intermediates. *Chem. Rev.* **2004**, *104*, 939−986.
(12) Solomon, E. I.; Decker, A.; Lehnert, N. Non-heme Iron Enzymes: Contrasts to Heme Catalysis. *Proc. Natl. Acad. Sci. U. S. A.* **2003**, *100*, 3589−3594.
(13) Bruijnincx, P. C. A.; van Koten, G.; Klein Gebbink, R. J. M. Mononuclear Non-heme Iron Enzymes with the 2-His-1caboxylate Facial Triad: Recent Developments in Enzymology and Modeling Studies. *Chem. Soc. Rev.* **2008**, *37*, 2716−2744.
(14) Kovaleva, E. G.; Lipscomb, J. D. Versatility of Biological Non-heme Fe(II) Centers in Oxyden Activation Reactions. *Nat. Chem. Biol.* **2008**, *4*, 186−193.
(15) Mbughuni, M. M.; Lipscomb, J. D. In *Encyclopedia of Metalloproteins*; Uversky, V. N., Kretsinger, R. H., Permyakov, E. A., Eds.; Springer Science: New York, 2013; pp 1006−1015.
(16) Thelander, L.; Reichard, P. Reduction of Ribonucleotides. *Annu. Rev. Biochem.* **1979**, *48*, 133−158.
(17) Fontecave, M.; Nordlund, P.; Eklund, H.; Reichard, P. The Redox Centers of Ribonucleotide Reductase of Escherichia Coli. *Adv. Enzymol. Relat. Areas Mol. Biol.* **2006**, *65*, 147−183.
(18) Harlos, K.; Schofield, C. J.; Zhang, Z.; Ren, J.; Stammers, D. K.; Baldwin, J. E. Structural Origins of the Selectivity of the Trifunctional Oxygenase Clavaminic Acid Synthase. *Nat. Struct. Biol.* **2000**, *7*, 127−133.
(19) Han, S.; Eltis, L. D.; Timmis, K. N.; Muchmore, S. W.; Bolin, J. T. Crystal Structure of the Biphenyl-cleaving Extradiol Dioxygenase from a PCB-degrading Pseudomonad. *Science* **1995**, *270*, 976−980.
(20) Shannon, R. D. Revised Effective Ionic Radii and Systematic Studies of Interatomic Distances in Halides and Chalcogenides. *Acta Crystallogr., Sect. A: Cryst. Phys., Diffr., Theor. Gen. Crystallogr.* **1976**, *32*, 751−767.
(21) Irving, H.; Williams, R. J. P. Order of Stability of Metal Complexes. *Nature* **1948**, *162*, 746−747.
(22) Dudev, T.; Lim, C. Competition among Metal Ions for Protein Binding Sites: Determinants of Metal Ion Selectivity in Proteins. *Chem. Rev.* **2014**, *114*, 538−556.
(23) Dudev, T.; Lim, C. Ion Selectivity Strategies of Sodium Channel Selectivity Filters. *Acc. Chem. Res.* **2014**, *47*, 3580−3587.
(24) Dudev, T.; Lim, C. Factors Governing the Na+ vs K+ Selectivity in Sodium Ion Channels. *J. Am. Chem. Soc.* **2010**, *132*, 2321−2332.
(25) Kuppuraj, G.; Dudev, M.; Lim, C. Factors Governing Metal-ligand Distances and Coordination Geometries of Metal Complexes. *J. Phys. Chem. B* **2009**, *113*, 2952−2960.
(26) Dudev, T.; Lim, C. Competition between Li+ and Mg2+ in Metalloproteins. Implications for Lithium Therapy. *J. Am. Chem. Soc.* **2011**, *133*, 9506−9515.
(27) Dudev, T.; Lim, C. Competition among Ca2+, Mg2+, and Na+ for Model Ion Channel Selectivity Filters: Determinants of Ion Selectivity. *J. Phys. Chem. B* **2012**, *116*, 10703−10714.
(28) Dudev, T.; Lim, C. The Effect of Metal Binding on the Characteristic Infrared Band Intensities of Ligands of Biological Interest. *J. Mol. Struct.* **2012**, *1009*, 83−88.
(29) Dudev, T.; Lim, C. Importance of Metal Hydration on the Selectivity of Mg^{2+} versus Ca^{2+} in Magnesium Ion Channels. *J. Am. Chem. Soc.* **2013**, *135*, 17200−17208.
(30) Dudev, T.; Lim, C. Ion Selectivity in the Selectivity Filters of Acid-sensing Ion Channels. *Sci. Rep.* **2015**, *5*, 7864.
(31) Dudev, T.; Musset, B.; Morgan, D.; Cherny, V. V.; Smith, S. M. E.; Mazmanian, K.; DeCoursey, T. E.; Lim, C. Selectivity Mechanism of the Voltage-gated Proton Channel, HV1. *Sci. Rep.* **2015**, *5*, 10320.
(32) Dudev, T.; Mazmanian, K.; Lim, C. Factors Controlling the Selectivity for Na^{+} over Mg^{2+} in Sodium Transporters and Enzymes. *Phys. Chem. Chem. Phys.* **2016**, *18*, 16986−16997.
(33) Nikolova, V.; Angelova, S.; Markova, N.; Dudev, T. Gallium as a Therapeutic Agent: A Thermodynamic Evaluation of the Competition between Ga3+ and Fe3+ Ions in Metalloproteins. *J. Phys. Chem. B* **2016**, *120*, 2241−2248.
(34) Marcus, Y. Ionic Radii in Aqueous Solutions. *Chem. Rev.* **1988**, *88*, 1475−1498.
(35) Dudev, M.; Wang, J.; Dudev, T.; Lim, C. Factors Governing the Metal Coordination Number in Metal Complexes from Cambridge Structural Database Analyses. *J. Phys. Chem. B* **2006**, *110*, 1889−1895.
(36) Costas, M.; Mehn, M. P.; Jensen, M. P.; Que, L., Jr. Dioxygen Activation at Mononuclear Nonheme Iron Active Sites: Enzymes, Models, and Intermediates. *Chem. Rev.* **2004**, *104*, 939−986.
(37) Cotton, F. A.; Wilkinson, G. *Advanced Inorganic Chemistry*; Wiley: New York, 1980.
(38) Zhao, Y.; Truhlar, D. G. The M06 suite of density functionals for main group thermochemistry, thermochemical kinetics, noncovalent interactions, excited states, and transition elements: Two new functionals and systematic testing of four M06-class functionals and 12 other functionals. *Theor. Chem. Acc.* **2008**, *120*, 215−241.
(39) Frisch, M. J.; Trucks, G. W.; Schlegel, H. B.; Scuseria, G. E.; Robb, M. A.; Cheeseman, J. R.; Scalmani, G.; Barone, V.; Mennucci, B.; Petersson, G. A.; Nakatsuji, H.; Caricato, M.; Li, X.; Hratchian, H. P.; Izmaylov, A. F.; Bloino, J.; Zheng, G.; Sonnenberg, J. L.; Hada, M.; Ehara, M.; Toyota, K.; Fukuda, R.; Hasegawa, J.; Ishida, M.; Nakajima, T.; Honda, Y.; Kitao, O.; Nakai, H.; Vreven, T.; Montgomery, J. A., Jr.; Peralta, J. E.; Ogliaro, F.; Bearpark, M.; Heyd, J. J.; Brothers, E.; Kudin, K. N.; Staroverov, V. N.; Kobayashi, R.; Normand, J.; Raghavachari, K.; Rendell, A.; Burant, J. C.; Iyengar, S. S.; Tomasi, J.; Cossi, M.; Rega, N.; Millam, J. M.; Klene, M.; Knox, J. E.; Cross, J. B.; Bakken, V.; Adamo, C.; Jaramillo, J.; Gomperts, R.; Stratmann, R. E.; Yazyev, O.; Austin, A. J.; Cammi, R.; Pomelli, C.; Ochterski, J. W.; Martin, R. L.; Morokuma, K.; Zakrzewski, V. G.; Voth, G. A.; Salvador, P.; Dannenberg, J. J.; Dapprich, S.; Daniels, A. D.; Farkas, O.; Foresman, J. B.; Ortiz, J. V.; Cioslowski, J.; Fox, D. J. *Gaussian 09*; Gaussian, Inc., Wallingford, CT, 2009.
(40) Li, L.; Li, C.; Zhang, Z.; Alexov, E. On the Dielectric Constant of Proteins: Smooth Dielectric Function for Macromolecular Modeling and Its Implementation in DelPhi. *J. Chem. Theory Comput.* **2013**, *9*, 2126−2136.
(41) Mertz, E. L.; Krishtalik, L. I. Low dielectric response in enzyme active site. *Proc. Natl. Acad. Sci. U. S. A.* **2000**, *97*, 2081−2086.
(42) Zheng, J.; Thruhlar, D. G. Unpublished results, 2014.
(43) Marenich, A. V.; Cramer, C. J.; Truhlar, D. G. Universal Solvation Model Based on Solute Electron Density and on a Continuum Model of the Solvent Defined by the Bulk Dielectric Constant and Atomic Surface Tensions. *J. Phys. Chem. B* **2009**, *113*, 6378−6396.
(44) Dudev, T.; Lim, C. Determinants of K^{+} vs Na^{+} Selectivity in potassium channels. *J. Am. Chem. Soc.* **2009**, *131*, 8092−8101.
(45) Dudev, T.; Lim, C. A DFT/CDM Study of Metal-Carboxylate Interactions in Metalloproteins: Factors Governing the Maximum

DOI: 10.1021/acs.inorgchem.6b01822
Inorg. Chem. 2016, 55, 12644−12650

Number of Metal-Bound Carboxylates. *J. Am. Chem. Soc.* **2006**, *128*, 1553−1561.
(46) Sham, T. K.; Hastings, J. B.; Perlman, M. L. Structure and Dynamic Behavior of Transition-metal Ions in Aqueous Solution: an EXAFS Study of Electron-exchange Reactions. *J. Am. Chem. Soc.* **1980**, *102*, 5904−5906.
(47) Smith, R. M.; Martell, A. E. Critical Stability Constants, Enthalpies and Entropies for the Formation of Metal Complexes of Aminopolycarboxylic Acids and Carboxylic Acids. *Sci. Total Environ.* **1987**, *64*, 125−147.
(48) Sjoberg, S. Critical Evaluation of Stability Constants of Metal-Imidazole and Metal-Histamine Systems. *Pure Appl. Chem.* **1997**, *69*, 1549−1570.
(49) Dudev, T.; Lim, C. Tetrahedral vs. Octahedral Zn^{2+} Complexes with Ligands of Biological Interest: a DFT/CDM Study. *J. Am. Chem. Soc.* **2000**, *122*, 11146−11153.
(50) Anjem, A.; Varghese, S.; Imlay, J. A. Manganese Import is a Key Element of the OxyR Response to Hydrogen Peroxide in Escherichia Coli. *Mol. Microbiol.* **2009**, *72*, 844−858.
(51) Campos-Bermudez, V. A.; Leite, N. R.; Krog, R.; Costa-Filho, A. J.; Soncini, F. C.; Oliva, G.; Vila, A. J. Biochemical and Structural Characterization of Salmonella Typhimurium Glyoxalase II: New Insights into Metal Ion Selectivity. *Biochemistry* **2007**, *46*, 11069−11079.
(52) Anjem, A.; Imlay, J. A. Mononuclear Iron Enzymes are Primary Targets of Hydrogen Peroxide Stress. *J. Biol. Chem.* **2012**, *287*, 15544−15556.
(53) Sobota, J. M.; Imlay, J. A. Iron Enzyme Ribulose-5-phosphate 3-epimerase in Escherichia Coli is Rapidly Damaged by Hydrogen Peroxide but can be Protected by Manganese. *Proc. Natl. Acad. Sci. U. S. A.* **2011**, *108*, 5402−5407.
(54) Gattis, S. G.; Hernick, M.; Fierke, C. A. Active Site Metal Ion in UDP-3-O-((R)-3-Hydroxymyristoyl)-N-acetylglucosamine Deacetylase (LpxC) Switches between Fe(II) and Zn(II) Depending on Cellular Conditions. *J. Biol. Chem.* **2010**, *285*, 33788−33796.
(55) Hernick, M.; Gattis, S. G.; Penner-Hahn, J. E.; Fierke, C. A. Activation of E. coli UDP-3-O-(R-3-hydroxymyristoyl)-N-acetylglucosamine Deacetylase by Fe^{2+} Yields a More Efficient Enzyme with Altered Ligand Affinity. *Biochemistry* **2010**, *49*, 2246−2255.
(56) Kim, B.; Pithadia, A. S.; Fierke, C. A. Kinetics and Thermodynamics of Metal-binding to Histone Deacetylase 8. *Protein Sci.* **2015**, *24*, 354−365.
(57) Dowling, D. P.; Gattis, S. G.; Fierke, C. A.; Christianson, D. W. Structures of Metal-Substituted Human Histone Deacetylase 8 Provide Mechanistic Inferences on Biological Function. *Biochemistry* **2010**, *49*, 5048−5056.
(58) Becker, A.; Schlichting, I.; Kabsch, W.; Groche, D.; Schultz, S.; Wagner, A. F. Iron Center, Substrate Recognition, and Mechanism of Peptide Deformylase. *Nat. Struct. Biol.* **1998**, *5*, 1053−1058.
(59) Zhu, J.; Dizin, E.; Hu, X.; Wavreille, A.-S.; Park, J.; Pei, D. S-Ribosylhomocysteinase (LuxS) is a Mononuclear Iron Protein. *Biochemistry* **2003**, *42*, 4717−4726.
(60) Wu, R.; Wang, S.; Zhou, N.; Cao, Z.; Zhang, Y. A Proton-Shuttle Reaction Mechanism for Histone Deacetylase 8 and the Catalytic Role of Metal Ions. *J. Am. Chem. Soc.* **2010**, *132*, 9471−9479.

DOI: 10.1021/acs.inorgchem.6b01822
Inorg. Chem. 2016, 55, 12644−12650